Chinese Chemical Letters 32 (2021) 3095–3098

Contents lists available at ScienceDirect

Chinese Chemical Letters

journal homepage: www.elsevier.com/locate/cclet

Communication

A highly stable terbium metal-organic framework for efficient detection of picric acid in water

Zi-Ying Li[a], Zhao-Quan Yao[a], Rui Feng[b], Ming-Hua Sun[b], Xiao-Tian Shan[b], Zi-Hao Su[b], Wei Li[a,*], Xian-He Bu[a,b,*]

[a] TKL of Metal and Molecule Based Material Chemistry & School of Materials Science and Engineering, Tianjin 300350, China
[b] State Key Laboratory of Elemento-Organic Chemistry, College of Chemistry, Tianjin 300071, China

ARTICLE INFO

Article history:
Received 10 January 2021
Received in revised form 3 February 2021
Accepted 1 March 2021
Available online 4 March 2021

Keywords:
Metal-organic framework
Detection
Nitro aromatics
Picric acid
Fluorescent

ABSTRACT

A highly stable fluorescent terbium MOF ($Tb_4(paip)_6{\cdot}1.2H_2O$, paip = 5-(1*H*-pyrazole-4-yl)isophthalate) showing a sharp green emission (545 nm) and a quantum yield of 21.0% was successfully synthesized. This compound is shown to be a recyclable sensor for detecting picric acid in aqueous solution with both high sensitivity and selectivity, attributed to the electron transfer quenching mechanism.

As the most commonly used ingredients of explosives and intermediates of the industrial commodity, nitro aromatics have brought a multitude of security issues to our daily life [1,2]. Among these nitro compounds, picric acid (PA) has received particular attention in national security, military fields and environmental pollution due to its high explosive power and toxicity [3–5]. To date, the detection methods of picric acid include infrared and Raman spectroscopies [6], X-ray imaging techniques [7], fluorescence sensing [8–16], *etc*. Notably, fluorescence sensing, owing to its advantages of simplicity, high sensitivity, and rapid detection response, has been developed as a very promising technique.

To achieve efficient detection, luminescent probing materials with high sensitivity and selectivity to PA are highly thought after. Luminescent metal-organic frameworks (LMOFs) have great potential in sensing nitro aromatics due to their tuneable compositions, diverse structures, and high porosity [17–22]. A number of MOFs have been applied to detect PA [23–26], however, most of them are unable to function in water. In addition, PA shows strong acidity and may cause severe structural collapse, which places higher requirements on the stability and detection capability of MOF probes. In this regard, developing PA detecting MOFs with high water and pH stability remains a challenge. Lanthanide MOFs possess high stability and environmental resistance by virtue of large coordination numbers and high metal valence states [27–29]. Therefore, they have advantages as PA probes in aqueous solution. In addition, they have virtues of narrow emission bands, large storks shifts, and long lifetimes which are beneficial for luminescent probing [30–32]. Based on the above consideration, we herein report a new terbium MOF $Tb_4(paip)_6{\cdot}2H_2O$ (**NKU-130**), which can efficiently sense PA in water with high sensitivity, excellent selectivity as well as remarkable recyclability. More importantly, the efficient detection of PA can be realized in the presence of other nitro explosive interferences.

NKU-130 was synthesized by reacting $Tb(NO_3)_3{\cdot}6H_2O$ and electron rich π-conjugated H_2L (5-(1*H*-pyrazole-4-yl)isophthalic acid) in the hydrothermal conditions. It displays a three-dimensional network with one-dimensional triangular channels and its connectivity can be described as *stp* topology. It is worth noting that **NKU-130** possesses high stabilities in boiling water for one week and even in acidic/alkaline solutions for over 300 days. Meanwhile, **NKU-130** emits characteristic narrow peaks at 489, 545, 585 and 624 nm under 365 nm excitation due to the antenna effect of the ligand.

Single crystal X-ray diffraction results reveal **NKU-130** crystalizes in the *P3c1* space group and powder X-ray diffraction (PXRD) of synthesized crystals affirmed the phase purity (Fig. S6 in Supporting information). The crystallographic data were summarized in Tables S1 and S2 (Supporting information). The minimum

* Corresponding authors at: TKL of Metal and Molecule Based Material Chemistry & School of Materials Science and Engineering, Tianjin 300350, China.
E-mail addresses: wl276@nankai.edu.cn (W. Li), buxh@nankai.edu.cn (X.-H. Bu).

https://doi.org/10.1016/j.cclet.2021.03.008

asymmetric unit contains two thirds crystallographic independent Tb atoms and one ligand. Both Tb1 and Tb2 are 9-coordinated by O atoms, and the neighbouring Tb1 or Tb2 atoms are connected by three bridging μ_2-O atoms from carboxylate groups to form rod-like [Tb(COO)$_3$] SBUs (Fig. 1a). The free program SHAPE 2.0 suggests that the proximate ideal geometry of the nine-coordinated Tb1 and Tb2 is spherical tricapped trigonal prism (STTP), and their τ values have been listed in Table S3 (Supporting information). The rod SBUs of Tb1 and Tb2 are alternatively arranged and these atoms exhibit different spiral directions. The connecting *m*-phthalate groups between rod SBUs exhibit a two-fold disorder respectively towards inner and outer orientations along the c-axis (Fig. 1b). The pending electron-rich pyrazolyl groups of ligands are towards the inside of the aperture, which leads to a pore shape alteration from original hexagonal to triangular and an aperture reduction to 4.0 Å (Fig. 1c). The space-filling model of the trigonal channel is shown in Fig. 1d. From the topological point of view, when simplifying the ligand as a 4-connected node, the single 3D framework of **NKU-130** can then be viewed as a 4,6-connected stp net with the point symbol of $\{4.6^2\}_3\{4^6.6^3.8^6\}$ (Fig. S7 in Supporting information).

Considering the requirements for thermal stability of MOFs in fluorescent detection, thermogravimetric analysis (TGA) was carried out. The bulk crystals of **NKU-130** were soaked into DMF and EtOH separately for three days, dried in vacuum at 100 °C and TGA was performed subsequently under Ar atmosphere. The TGA curve (Fig. S10 in Supporting information) indicates a slight weight loss under 150 °C, which demonstrated the removal of guest solvents in minuscule channels. Meanwhile, the curve shows a platform before 540 °C, manifesting a remarkably high thermal stability. Variable-temperature powder XRD measurements demonstrated that the framework of **NKU-130** could remain stable up to 400 °C (Fig. S11 in Supporting information).

The solvent and pH stability of **NKU-130** was verified by PXRD measurements. As shown in Fig. S12 (Supporting information), the as-synthesized crystals were immersed in several common solvents (including DMF, DMAc, ethyl acetate, acetone, dichloromethane, methanol, tetrahydrofuran and water) for 7 days. The PXRD patterns are consistent well with the simulated one, indicating excellent resistance ability to multiple solvents. The stabilities in aqueous solution with different pH values were also performed, and **NKU-130** was proved to maintain its crystallinity between pH 3–12 even after 300 days (Fig. 2). Benefit from its thermal and pH stabilities, **NKU-130** can be a candidate material for fluorescent detection in the liquid phase under harsh conditions.

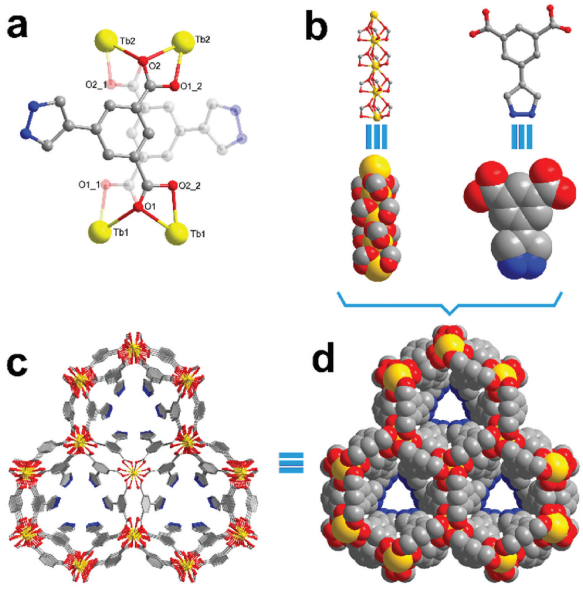

Fig. 1. (a) The asymmetric unit of **NKU-130**, A = -x + y, y, 1/2+z; B = 1-x + y, y, -1/2+z. The numbers after underline in atom labels represent for different sets of disorder structures. Yellow: Tb, red: O, blue: N, grey: C. (b) The rod SBU of [Tb(COO)$_3$] and ligand. (c) View of the 3D framework structure of **NKU-130** along the c-axis. (d) Space-filling model of **NKU-130**.

The photoluminescence (PL) spectra and fluorescence quantum yield of **NKU-130** in the solid state were measured at room temperature (Fig. S13 in Supporting information). The sharp peaks in PL spectra observed at 489, 545, 585 and 624 nm can be assigned to the $^5D_0 \rightarrow {}^7F_1$, $^5D_0 \rightarrow {}^7F_2$, $^5D_0 \rightarrow {}^7F_3$ and $^5D_0 \rightarrow {}^7F_4$ transitions, respectively, which are attributed to the antenna effect and characteristic f-f emission bands [33–35]. Fluorescence quantum yield of **NKU-130** in the solid state was calculated to be 21.0%. In addition, the PL spectra of **NKU-130** dispersed in H_2O and DMF also possess strong emission at 545 nm when excited at 327 nm.

To characterize the trace-quantity sensing ability towards nitro explosives, fluorescence titrations were performed with the incremental addition of analytes to **NKU-130** dispersed in water (Fig. 3). After incremental addition of PA solution (1×10^{-3} mol/L), rapid and high fluorescence quenching was observed with the naked eyes. As shown in Fig. 3a, the bright green emission of **NKU-130** sharply weakens with gradually adding PA solution. For illustrating the selectivity of detecting PA, fluorescence quenching efficiencies were also performed with other nitro aromatics, such as 1,4-dinitrobenzene (1,4-DNB), 2,6-dinitrotoluene (2,6-DNT), 1,3-dinitrobenzene (1,3-DNB) and nitrobenzene (NB). As shown in Fig. S14 (Supporting information), with the dropping of diverse nitro explosives at the concentration of 2.5×10^{-3} mol/L, the fluorescence of **NKU-130** could still be observed. The remaining nitro explosives have almost no quenching effect, indicating that **NKU-130** has a high PA selectivity (Fig. S15 in Supporting information).

Affected by the selective quenching effect, we also performed luminescence quenching titration with low concentration PA, thus obtaining the detection limit of PA. The fluorescence quenching efficiency was analyzed by the Stern-Volmer (SV) equation, $(I_0/I) = K_{sv}[A] + 1$, where I_0 and I are the initial fluorescence intensity before and after the analyte is added, respectively. [A] is the molar concentration of the analyte, and K_{sv} is the quenching constant (L/mol) [36–38]. At low concentrations, the SV plot of PA is almost linear. The quenching constant for PA was calculated to be 2.012×10^4 L/mol from the direct fitting of the plot, which demonstrates the high quenching capability of **NKU-130** toward PA. The calculated detection limit is 1.3×10^{-5} mol/L (3 ppm). Besides, we also carried out the titration experiments to

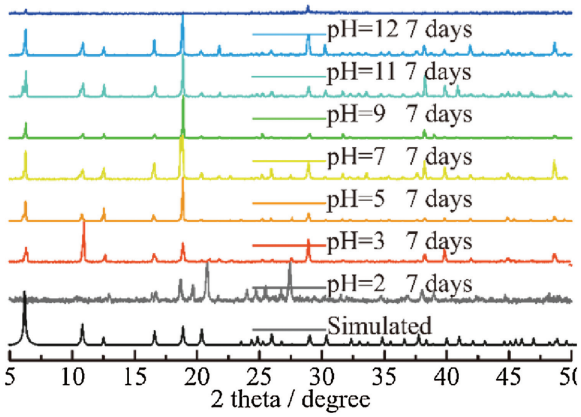

Fig. 2. PXRD patterns for **NKU-130** immersed in aqueous solutions (pH 2–13) and exposed in air.

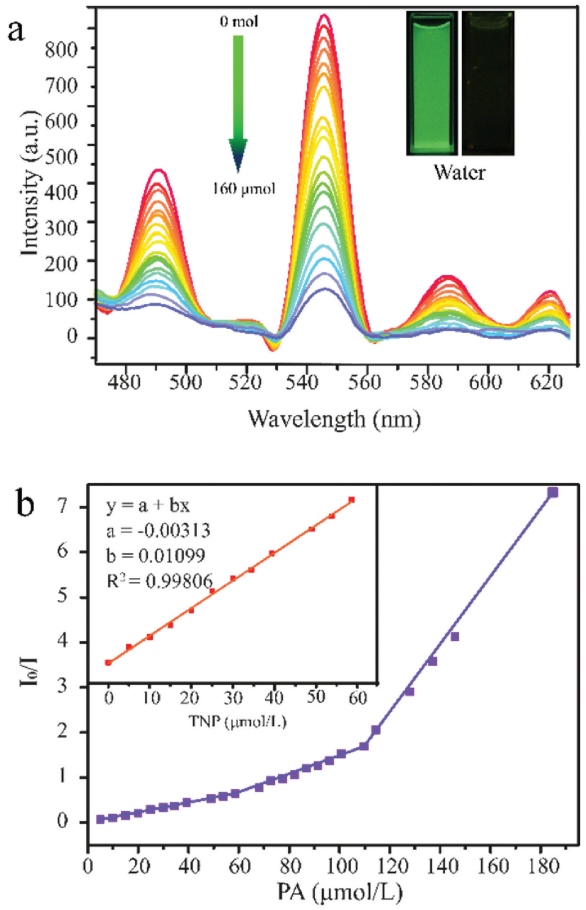

Fig. 3. (a) Emission spectra of **NKU-130** suspension in water treated with different concentrations of PA. (b) Stern-Volmer plot of I_0/I *vs.* the concentration of PA in aqueous solution.

investigate the recyclability and immediate responsiveness of **NKU-130** (Figs. S14 and S16 in Supporting information). Even after twenty cycles, it remains good quenching strength at a concentration of 10^{-3} mol/L. The PXRD spectrum shows it maintains crystalline after the sensing experiments (Fig. S17 in Supporting information). Similar fluorescence experiments were also taken for the suspensions in DMF and the results show that the sensitivity and recyclability in DMF of **NKU-130** are reminiscent of those in water (Fig. S18 in Supporting information). Furthermore, in order to verify the practical use of **NKU-130** as a sensor for PA detection, the luminescent paper-based visual sensors were prepared. The filter papers were prepared by filtering the suspension of **NKU-130** (10 mg) in water (10 mL) [39]. It showed that the fluorescence intensity of the test paper changes significantly before and after the addition of PA, demonstrating it could be applied conveniently (Fig. S19 in Supporting information).

To fully understand the quenching behavior of **NKU-130** in the presence of PA, the quenching mechanism needs to be well corroborated. Common fluorescence quenching mechanisms include structural collapse, energy resonance theory (RET) and photo-induced electron transfer (PET) [31,40,41]. Firstly, PXRD pattern of the powder sample after recycling test showed that the framework structure was intact during the detection process, which excludes the decomposition induced fluorescence quenching mechanism [42]. Secondly, the fluorescence resonance energy transferred from the fluorophore to the analyte might be one reason for the quenching process [43]. However, the UV–vis adsorption of nitro explosives and **NKU-130** shows negligible overlap, which rules out this possibility (Fig. S20 in Supporting information). The observed overlap between the absorption band of the nitro explosives and the excitation band of the sensing **MOF-130** indicates there is a competitive adsorption mechanism (Fig. S21 in Supporting information). With an excitation wavelength of 327 nm, PA has a much stronger absorption over other explosives. This electronic characteristic of PA results in lower absorbance of the ligand and lower energy transfer from the ligand to Tb^{3+} ion, hence ultimately leading to the fluorescence quenching. Thirdly, photo-induced electron transfer (PET) can also contribute to the fluorescence quenching process. The lower the lowest unoccupied orbit (LUMO), the more likely the process of photogenic electron transfer will occur. Since the LUMOs of PA are lower compared to those from other nitro compounds (PA < 1,4-DNB < 1,3-DNB < 2,6-DNT < NB), and electron transfer from **NKU-130** to PA is more likely to process to result in the sudden extinction (Figs. 4a and b). Considering the aforementioned two latter factors, it can be concluded that the competitive absorption of excitation light energy and electronic interactions between PA and ligands largely affect the ligand-to-metal energy transfer process, thus bursting the characteristic emission of Tb^{3+} ions. The non-linear SV curves also indicate the existence of both static and dynamic bursting mechanisms in the process (Fig. 4c).

In conclusion, we have successfully synthesized a highly thermal and water stable terbium MOF (**NKU-130**) which emits strong green light with a high quantum yield of 21.0%. Notably, **NKU-130** can be utilized for quick and sensitive PA detection through fluorescence quenching and the mechanism is attributed to the cooperative electron transfer and competitive adsorption. The high stability and recyclability of **NKU-130** make it a potential material candidate for sensing PA in harsh conditions.

Declaration of competing interest

The authors declare that they have no known competing financial interests or personal relationships that could have appeared to influence the work reported in this paper.

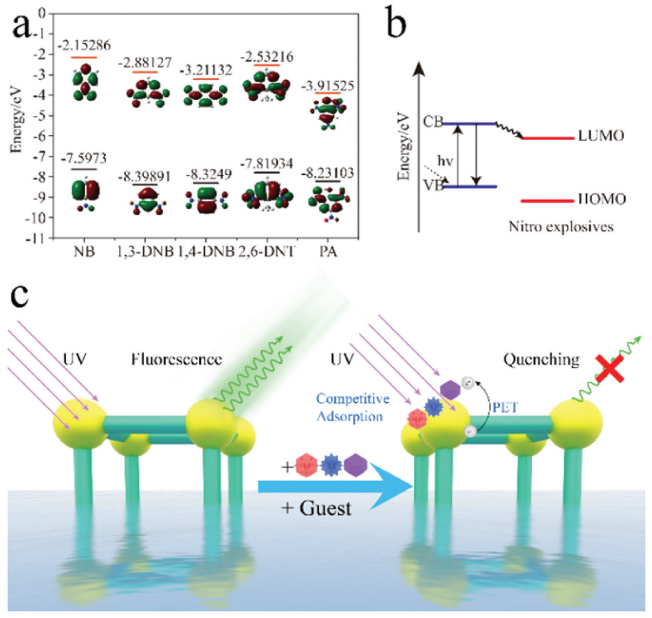

Fig. 4. (a) HOMO and LUMO energies for calculated nitro aromatics by using the B3LYP/6-31 G(d,p) level of theory. (b) Schematic representation of the PET process. (c) The quenching mechanism for detecting PA by **NKU-130**.

Acknowledgments

This work was supported by the National Natural Science Foundation of China (NSFC, Nos. 22035003, 91856124, 22001132 and 19JCZDJC37200) and China Postdoctoral Science Foundation (No. 2019M651011).

Appendix A. Supplementary data

Supplementary material related to this article can be found, in the online version, at doi:https://doi.org/10.1016/j.cclet.2021.03.008.

References

[1] Y. Zhang, S. Yuan, G. Day, et al., Coord. Chem. Rev. 354 (2018) 28–45.
[2] Z. Hu, B.J. Deibert, J. Li, Chem. Soc. Rev. 43 (2014) 5815–5840.
[3] Z.Q. Shi, Z.J. Guo, H.G. Zheng, Chem. Commun. 51 (2015) 8300–8303.
[4] S. Shanmugaraju, C. Dabadie, K. Byrne, et al., Chem. Sci. 8 (2017) 1535–1546.
[5] M. Rong, L. Lin, X. Song, et al., Anal. Chem. 87 (2015) 1288–1296.
[6] J.S. Caygill, F. Davis, S.P.J. Higson, Talanta 88 (2012) 14–29.
[7] K. Wells, D.A. Bradley, Appl. Radiat. Isotopes 70 (2012) 1729–1746.
[8] Z.H. Fu, Y.W. Wang, Y. Peng, Chem. Commun. 53 (2017) 10524–10527.
[9] M. Partha Sarathi, S. Sankarasekaran, Chem. Commun. (2015) 16014–16032.
[10] D. Bai, M.H. Huynh, D.A. Simpson, et al., APL Mater. 8 (2020) 081102.
[11] J.R. Harwell, J.M.E. Glackin, N.J.L.K. Davis, et al., APL Mater. 8 (2020) 071106.
[12] Z.Q. Yao, J. Xu, B. Zou, et al., Angew. Chem. Int. Ed. 58 (2019) 5614–5618.
[13] X.P. Wang, L.L. Han, Z. Wang, et al., J. Mol. Struct. 1107 (2016) 1–6.
[14] W.M. Chen, X.L. Meng, G.L. Zhuang, et al., J. Mater. Chem. A 5 (2017) 13079–13085.
[15] X.M. Tian, S.L. Yao, C.Q. Qiu, et al., Inorg. Chem. 59 (2020) 2803–2810.
[16] S.L. Yao, S.J. Liu, X.M. Tian, et al., Inorg. Chem. 58 (2019) 3578–3581.
[17] I. Stassen, N.C. Burtch, A.A. Talin, et al., Chem. Soc. Rev. 46 (2017) 3185–3241.
[18] S. Wu, H. Min, W. Shi, P. Cheng, Adv. Mater. 32 (2020) 1805871.
[19] S. Yuan, L. Feng, K. Wang, et al., Adv. Mater. 30 (2018) 1704303.
[20] Z.Q. Yao, G.Y. Li, J. Xu, et al., Chem. Eur. J. 24 (2018) 3192–3198.
[21] D. Lei, N. Liu, T. Su, et al., APL Mater. 8 (2020) 110702.
[22] K. Chen, C. Wu, Chin. Chem. Lett. 29 (2018) 823–826.
[23] X.J. Hong, Q. Wei, Y.P. Cai, et al., ACS Appl. Mater. Interfaces 9 (2017) 4701–4708.
[24] P. Ju, E.S. Zhang, X. Wang, et al., Chin. J. Struct. Chem. 38 (2019) 1578–1584.
[25] Y. Jiang, L. Sun, J. Du, et al., Cryst. Growth Des. 17 (2017) 2090–2096.
[26] S. Wu, Y. Lin, J. Liu, et al., Adv. Funct. Mater. 28 (2018) 1707169.
[27] B. Yan, Acc. Chem. Res. 50 (2017) 2789–2798.
[28] S. Abednatanzi, P.G. Derakhshandeh, H. Depauw, et al., Chem. Soc. Rev. 48 (2019) 2535–2565.
[29] P. Mahata, S.K. Mondal, D.K. Singha, P. Majee, Dalton Trans. 46 (2017) 301–328.
[30] W. Liu, X. Huang, C. Chen, et al., Chem. Eur. J. 25 (2019) 1090–1097.
[31] W. Liu, X. Huang, C. Xu, et al., Chem. Eur. J. 22 (2016) 18769–18776.
[32] P. Wu, L. Xia, M. Huangfu, et al., Inorg. Chem. 59 (2020) 264–273.
[33] G. Wang, Q. Peng, Y. Li, Acc. Chem. Res. 44 (2011) 322–332.
[34] Y. Cui, H. Xu, Y. Yue, et al., J. Am. Chem. Soc. 134 (2012) 3979–3982.
[35] F. Wang, Y. Han, C.S. Lim, et al., Nature 463 (2010) 1061–1065.
[36] R. Goswami, S.C. Mandal, B. Pathak, S. Neogi, ACS Appl. Mater. Interfaces 11 (2019) 9042–9053.
[37] K. Xing, R. Fan, J. Wang, et al., ACS Appl. Mater. Interfaces 9 (2017) 19881–19893.
[38] S. Xing, Q. Bing, H. Qi, et al., ACS Appl. Mater. Interfaces 9 (2017) 23828–23835.
[39] K. Sheng, H. Lu, A. Sun, et al., Chin. Chem. Lett. 30 (2019) 895–898.
[40] B. Gui, X. Liu, G. Yu, et al., CCS Chemistry (2020) 2054–2062.
[41] B. Gui, Y. Meng, Y. Xie, et al., Adv. Mater. (2018) e1802329.
[42] X. Zhuang, N. Zhang, X. Zhang, et al., Microchem. J. 153 (2020) 104498.
[43] H.H. Yu, J.Q. Chi, Z.M. Su, et al., CrystEngComm 22 (2020) 3638–3643.